Journal of VLSI Signal Processing 30, 35–54, 2002


# Modulation and Coding for Noncoherent Communications*

MICHAEL L. McCLOUD AND MAHESH K. VARANASI
*Department of Electrical and Computer Engineering, University of Colorado at Boulder, Boulder, CO 80309-0425 USA*

*Received October 5, 2000; Revised July 23, 2001*

**Abstract.** Until recently, the theory of noncoherent communications was premised on the use of orthogonal multi-pulse modulation such as frequency shift keying. The main drawback of this modulation scheme has been its poor spectral efficiency (rate/bandwidth). This paper considers instead the more general non-orthogonal multi-pulse modulation (NMM) technique. Optimal and suboptimal noncoherent detection strategies for NMM are reviewed and their asymptotic (high SNR) performances are characterized for the additive Gaussian as well as the Rayleigh fading channels. The resulting non-Euclidean distance measures are then used to design NMM signal sets that yield significantly higher bandwidth efficiencies than their orthogonal counterparts. NMM in conjunction with convolutional coding is also studied as a way to improve energy efficiency. Several optimal convolutional codes are examined together with our signal designs. An introduction to equalization on the noncoherent channel is also presented and illustrated by example. This paper thus contains several new results and attempts at the same time to give a tutorial exposition of the subject of noncoherent communications.

**Keywords:** noncoherent communications, modulation, signal design, convolutional coding, error analysis

## 1. Introduction

Orthogonal multi-pulse modulation (OMM) is usually employed on noncoherent communication channels, in which a user transmits one of $M$ orthogonal signals during each baud interval. The most common implementation of OMM is frequency shift-keying (FSK), when the orthogonal signals are chosen to be $M$ truncated sinusoidal waveforms. Detection may be performed by correlating the received waveform with each sinusoid and then choosing the symbol that corresponds to the largest magnitude matched-filter output. The chief advantage of OMM is the simple implementation of the envelope detection receiver. Its main drawback is its poor spectral efficiency, requiring a bandwidth which grows exponentially with the transmission rate (number of information bits per baud interval).

*This work was supported in part by National Science Foundation Grants ANI-9725778 and ECS-9979400 and by US Army Research Office Grant DADD19-99-1-0291.

Non-orthogonal multi-pulse modulation (NMM) is a signaling scheme in which the signals are generally correlated. The primary advantage of NMM over OMM is that large signal sets may be designed with small bandwidth expenditures. When NMM signal sets are employed, the optimal detection rules for the noncoherent additive white Gaussian noise (AWGN) and Rayleigh fading channels have an asymptotic error rate performance that can be exploited for signal design. For equal-energy signals, the distance measure which dictates performance at large values of the signal to noise ratio (SNR) is the maximum magnitude of the cross-correlations between distinct pairs of (complex-valued) signals.

In this paper, we have attempted to present the subject of noncoherent communications in a comprehensive yet accessible manner. We develop a theory of detection, signal design, coding, and equalization for noncoherent communications with NMM. Our results on detectors and their performance analysis (Sections 3, 4) are presented primarily as review, as they

appear in the journal references [1, 2]. The equalization (Section 9) and NMM signal design (Section 5) results have appeared in conference versions of this paper in [3] and [4], respectively. Our findings on convolutional coding for NMM for the AWGN channel (Section 7) are new, as is the asymptotic analysis of the optimal noncoherent detector (Section 4.3). Also presented here for the first time are the results on detection and convolutional coding and performance analysis for the Rayleigh fading channel. For simplicity, we have restricted attention to single-antenna systems.

Signal detection on the noncoherent NMM channel is considered in Section 3. The dependence of the error probability for the AWGN channel on the signal geometry for both equal and unequal energy signal constellations is derived in Section 4. These results suggest the problem of designing signals for use on the noncoherent channel. In Section 5 we discuss signal design for the AWGN channel. In Section 5.1 we propose a method of successive updates to design equal energy NMM signal constellations with a guaranteed minimum distance in a fixed dimensional space [4]. A non-linear optimization problem is solved at each update subject to several quadratic inequality constraints. A modified Fletcher-Powell optimization algorithm is employed through the FSQP [5] optimization package. This design technique is versatile and able to handle arbitrary combinations of dimensionality and maximum cross-correlation. It has been found to work well for relatively small cardinality signal sets. In Section 5.2 we introduce signal designs for unequal energy constellations. We present a method based on building signals in disjoint energy shells and give an example that gives a notable improvement in energy efficiency over the equal energy designs.

To develop insight into the potential gains that can be expected from our NMM designs with coding, we obtain the capacity of the NMM channel in Section 6 by extending the corresponding OMM results of [6]. By manipulating the multi-dimensional integral expression for mutual information appropriately, we find an efficient Monte-Carlo procedure for numerically evaluating the channel capacity. We compare our designs with OMM through the coded spectral efficiency measure, which is simply the channel capacity normalized by the minimum signal bandwidth required. We find that our designs improve considerably on OMM.

The NMM signal sets are then used in conjunction with low-rate convolutional codes in Section 7 to map out new regions of the energy-spectral efficiency plane. We examine rate $1/Q$ convolutional codes presented for use with OMM in [7]. Numerical results indicate that by allowing correlation among the modulation waveforms, we can obtain improvements in the spectral efficiency with small losses in energy efficiency. We then outline the extension of our results to the Rayleigh fading channel in Section 8 for the single-transmit and single-receive antenna channel. The optimal rule admits an asymptotic performance measure which is identical to that found for the AWGN channel so the signal design results developed for that channel may be used without modification. We derive the two-codeword error probabilities (and their asymptotic behavior) for convolutional coding on this channel. The general case of multiple transmit antenna diversity is developed in [8, 9].

In the presence of a bandlimiting or multi-path channel, the orthogonality of the information bearing signals with OMM is lost and the received waveforms must be treated as resulting from NMM with intersymbol interference (ISI) regardless of the original modulation scheme. Equalization of such signals is described as difficult in [10]. However, in [11] several equalizers (linear and decision feedback) are proposed for NMM over baseband (*coherent*) channels. In Section IX we develop zero-forcing equalization for use with the multiple input/multiple output (MIMO) discrete time model characterizing NMM over the *noncoherent* ISI channel as in [3]. The more general case of the non-invertible channel is treated in [12, 13].

## 2. The Noncoherent Communication Channel

We begin with a description of the basic complex baseband communication system depicted in Fig. 1. A source transmits a sequence of M-ary information symbols $\{m_l\}_{l=-\infty}^{\infty}$, $m_l \in \{1, \ldots, M\}$, at rate $1/T$ symbols/sec. The modulator maps each input symbol, $m_l$, into one of $M$ possible waveforms. This transmitted signal may pass through a channel which may induce distortion, for instance when the transmit medium has a small bandwidth relative to the signal or when frequency selective fading is present. We model this distortion as resulting from a linear system with complex-baseband transfer function $H(f)$. The channel may also induce a time-varying fading of the signal in which case the amplitude and phase change due to multipath effects. Finally, additive noise corrupts the signal and the received waveform is

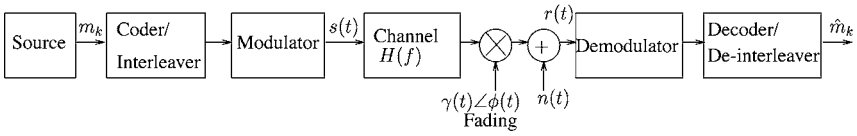


*Figure 1.* Communication system model.

$$r(t) = \gamma(t)e^{j\phi(t)} \sum_l \sqrt{E_{m_l}}\, s_{m_l}(t - lT) + n(t), \quad (1)$$

where $s_m(t)$ is the $m$th composite waveform corresponding to the response of the channel to the $m$th transmitted signal, each normalized to have unit energy. The additive noise, $n(t)$, is modeled as a complex circularly symmetric white Gaussian process, with power $\sigma^2$. In the special case of a distortionless channel ($H(f) = 1$ and $\gamma(t) = 1$), we say that we have the additive white Gaussian noise (AWGN) channel model. When we employ channel coding, we assume that perfect interleaving is employed so that the carrier phase and the fading process can be modeled as being independent from symbol to symbol.

In the absence of inter-symbol interference and fading we consider the simplified model for the noncoherent AWGN channel:

$$r(t) = \sqrt{E_m}\, e^{-j\phi_m} s_m(t) + n(t), \quad (2)$$

where we do not assume knowledge of the carrier phase $\phi_m$.

### 2.1. *Orthogonal and Non-Orthogonal Multipulse Modulation*

Orthogonal multipulse modulation (OMM) is often employed on noncoherent channels wherein one of $M$ time-limited orthogonal signals is transmitted at each baud period. The most common realization of OMM is frequency shift keying (FSK), wherein one of $M$ orthogonal sinusoids with frequency separation $\Delta f$ is transmitted at each baud period. Detection is performed by matching the received signal $r(t)$ against each low-pass equivalent transmitted signal, $s_m(t)$:

$$\hat{m} = \arg\max_m \left| \int_0^T r(t)\overline{s_m}(t)\, dt \right|^2. \quad (3)$$

The main drawback of OMM is its low spectral efficiency (the ratio of the transmission rate to the bandwidth employed). The smallest achievable bandwidth for OMM is $B = M/T$. This implies that as the transmission rate, $R = \log_2 M/T$, is increased, the spectral efficiency decreases as $\log_2(M)/M$. In order to overcome this problem, non-orthogonal multipulse modulation (NMM) may be employed, wherein the signals are allowed to be correlated. For a fixed signal dimensionality, $N$, we find that NMM employing $M$ signals has a spectral efficiency of $\log_2(M)/N$. For a fixed performance, this increase in spectral efficiency comes at the expense of an increase in transmitted power.

### 2.2. *Signal Space Representations*

Suppose that the NMM signals have a common basis, $\{u_n(t)\}_{n=1}^N$, meaning that every signal has the baseband representation

$$s_m(t) = \sum_{n=1}^{N} s_{m,n} u_n(t). \quad (4)$$

A consequence of the Karhunen–Loeve expansion theorem [14] is that for white noise, $n(t)$, the received signal, $r(t) = \sqrt{E_m}\, e^{j\phi_m} s_m(t) + n(t)$, may be projected onto this basis for the purpose of detection without loss of generality. This means that any receiver for the noncoherent channel can employ the front-end generalized sampler $G : \mathbb{L}^2 \to \mathbb{C}^N$ with

$$\{\mathbf{y}\}_n = \{G[r(t)]\}_n = \langle r(t), u_n(t)\rangle = \int r(t)u_n(t)\, dt. \quad (5)$$

The $N \times 1$ measurement vector $\mathbf{y}$ is termed a *sufficient statistic* for the detection problem. Assuming that the basis functions $\{u_n(t)\}$ satisfy the generalized Nyquist condition [10], we obtain an ISI-free model for $\mathbf{y}$ which, under hypothesis $H_m$ (that the $m$th signal is transmitted), is given as

$$\mathbf{y} = \alpha_m \mathbf{s}_m + \mathbf{n}, \quad (6)$$

where $\alpha_m = \sqrt{E_m}\, e^{j\phi_m}$ represents any amplitude and phase distortions due to a non-ideal channel. The signal vector, $\mathbf{s}_m$, is given by

$$\{\mathbf{s}_m\}_n = \langle s_m(t), u_n(t)\rangle, \tag{7}$$

and the additive noise, $\mathbf{n}$, is a complex normal random vector with mean zero and correlation $E[\mathbf{n}\mathbf{n}^*] = \sigma^2\mathbf{I}$.

Throughout this paper, finite dimensional vectors $\mathbf{x} \in \mathbb{C}^{N\times 1}$ and matrices $\mathbf{A} \in \mathbb{C}^{N\times M}$ are denoted by boldface type. We will use the notation $\mathbf{A}^*$ to denote the complex conjugate transpose of the matrix $\mathbf{A}$.

## 3. Detection

### 3.1. Generalized Maximum Likelihood Detection

The idea behind the generalized maximum likelihood (GML) detection strategy is that if the gain, $\alpha_m = \sqrt{E_m}\, e^{j\phi}$, were known to the receiver, the optimal decision rule would be the maximum likelihood (ML) detector:

$$\hat{m}_{ML} = \arg\min_m \|\mathbf{y} - \alpha_m \mathbf{s}_m\|^2, \tag{8}$$

assuming equal priors. This detector is derived from maximizing the likelihood functions

$$f_m(\alpha_m; \mathbf{y}) = (\pi\sigma^2)^{-N} \exp\left\{-\frac{1}{\sigma^2}\|\mathbf{y} - \alpha_m \mathbf{s}_m\|^2\right\} \tag{9}$$

over $m$. In the absence of this side information we may substitute the maximum likelihood estimate of $\alpha$ into the detector to form the GML rule

$$\hat{m}_{GML} = \arg\max_m f_m(\widehat{\alpha_m}; \mathbf{y}). \tag{10}$$

The maximum likelihood estimate is found from the standard least squares theory (see e.g. [15]) and is given by $\widehat{\alpha_m}\mathbf{s}_m = \mathbf{P}_{\mathbf{s}_m}\mathbf{y}$, where $\mathbf{P}_{\mathbf{s}_m} = \mathbf{s}_m\mathbf{s}_m^*$ is the orthogonal projection matrix with range space $\langle \mathbf{s}_m\rangle$. The corresponding non-coherent GML detection rule is

$$\hat{m}_{GML} = \arg\max_m |\mathbf{y}^*\mathbf{s}_m|^2, \tag{11}$$

and was derived in a different context in [1, 2].

### 3.2. The Asymptotically Optimal Detector

In this section we develop the asymptotically optimal rule of [1]. We assume knowledge of the signal energies, $\{E_m\}$, and look for the optimal detector for the unknown phase channel. Assuming that the phase has a uniform distribution, $U[0, 2\pi)$, the minimum error probability rule averages the likelihood functions over the distribution for phase and selects the maximum of the resulting statistics. The optimal detector is therefore

$$\begin{aligned}
\hat{m} &= \arg\max_{m\in\{1,\ldots,M\}} \left\{ \int_0^{2\pi} \frac{1}{(\pi\sigma^2)^N} \right. \\
&\qquad \left. \times \exp\left\{-\frac{1}{\sigma^2}\left\|\mathbf{y} - \sqrt{E_m}\, e^{j\phi_m}\mathbf{s}_m\right\|^2\right\}\frac{d\phi_m}{2\pi}\right\} \\
&= \arg\max_{m\in\{1,\ldots,M\}} \left\{ \exp\left\{-\frac{E_m}{\sigma^2}\right\} \int_0^{2\pi} \exp\left\{\frac{2\sqrt{E_m}}{\sigma^2}\right. \right. \\
&\qquad \left. \left. \times (|\mathbf{y}^*\mathbf{s}_m|\cos(\phi_m + \alpha_m))\right\}\frac{d\phi_m}{2\pi}\right\} \\
&= \arg\max_{i\in\{1,\ldots,M\}} \left\{ \exp\left\{-\frac{E_m}{\sigma^2}\right\} I_0\left(\frac{2\sqrt{E_m}|\mathbf{y}^*\mathbf{s}_m|}{\sigma^2}\right)\right\},
\end{aligned} \tag{12}$$

where $\alpha_m = \mathrm{Arg}(\mathbf{y}^*\mathbf{s}_m)$, $I_0(x)$ is the zeroth-order modified Bessel function of the first kind, and we have removed the hypothesis independent terms $1/(\pi\sigma^2)^N$ and $\exp\{-\mathbf{y}^*\mathbf{y}/\sigma^2\}$.

This test is optimal in terms of probability of error but may be too complex to implement due to the need to evaluate the Bessel function at the detector. For this reason we consider the asymptotically optimal (AO) approximation introduced in [16]:

$$\hat{m}_{AO} = \arg\max_{m\in\{1,\ldots,M\}} \{-E_m + 2\sqrt{E_m}|\mathbf{y}^*\mathbf{s}_m|\}. \tag{13}$$

This test was derived by using the asymptotic expansion of the Bessel function [17]

$$I_0(x) = \frac{\exp\{x\}}{\sqrt{2\pi x}}\left[1 + O\left(\frac{1}{x}\right)\right] \tag{14}$$

and ignoring the denominator terms.

It is interesting to notice that the AO detector is also a GML rule when the phase, $\phi_m$, is assumed unknown and the likelihood function of (9) is maximized with respect to $\phi_m$. Specifically, we first let

$$\begin{aligned}
\hat{\phi}_m &= \arg\max_{\phi_m\in[0,2\pi)} f_m(\mathbf{y}) \\
&= \arg\min_{\phi_m\in[0,2\pi)} \left\|\mathbf{y} - \sqrt{E_m}\, e^{j\phi_m}\mathbf{s}_m\right\|^2 \\
&= \arg\min_{\phi_m\in[0,2\pi)} -2\sqrt{E_m}|\mathbf{y}^*\mathbf{s}_m|\cos(\phi_m + \mathrm{Arg}[\mathbf{y}^*\mathbf{s}_m]) \\
&= -\mathrm{Arg}[\mathbf{y}^*\mathbf{s}_m].
\end{aligned} \tag{15}$$

The corresponding GML test is found by maximizing the likelihood functions of (9) over $m$ with the phase term replaced by the corresponding $\hat{\phi}_m$ for each hypothesis:

$$\begin{aligned}\hat{m} &= \arg\max_m f_m(\mathbf{y};\hat{\phi}_m)\\ &= \arg\min_m \left\|\mathbf{y}-\sqrt{E_m}\,e^{j\hat{\phi}_m}\mathbf{s}_m\right\|^2\\ &= \arg\min_m \left\{\|\mathbf{y}\|^2-\sqrt{E_m}\,\mathbf{y}^*\mathbf{s}_m e^{j\hat{\phi}_m}\right.\\ &\quad \left.-\sqrt{E_m}\,\mathbf{s}_m^*\mathbf{y}e^{-j\hat{\phi}_m}+E_m\right\}\\ &= \arg\max_m \left\{2\sqrt{E_m}|\mathbf{y}^*\mathbf{s}_m|-E_m\right\}, \end{aligned} \tag{16}$$

which is exactly the AO test of (13).

Finally, notice that when the signals have equal energy ($E_m$ is constant) the AO test reduces to the GML detector.

## 4. Performance Analysis of the Noncoherent Detectors

In this section we characterize the performance of the GML and AO detectors in terms of exact expressions for pair-wise error probabilities and study their asymptotic high signal-to-noise ratio (SNR) behavior for the noncoherent AWGN channel.

Given a detector, $\phi$, we can bound the probability of error by

$$\frac{1}{M}\max_{l\neq m} P^{\phi}(m,l) \le P^{\phi} \le \frac{1}{M}\sum_{m=1}^{M}\sum_{\substack{l=1\\ l\neq m}}^{M} P^{\phi}(m,l), \tag{17}$$

where $P^{\phi}(m,l)$ is the probability that signal $l$ is judged more likely than signal $m$ under hypothesis $H_m$ (that signal $m$ is transmitted). These bounds are asymptotically coincident in the SNR so that we need only characterize the pair-wise error probabilities $P^{\phi}(m,l)$.

In the next subsections and the sections to follow, we shall repeatedly use the $n$th order modified Bessel function, $I_n(x)$, and the Marcum $Q$ function $Q_1(a,b)$, defined by

$$\begin{aligned} I_n(z) &= \frac{1}{2\pi}\int_0^{2\pi} e^{\pm jn\theta}e^{z\cos(\theta)}\,d\theta\\ &= \sum_{k=0}^{\infty}\frac{(x/2)^{n+2k}}{k!(n+k)!}\end{aligned}$$

$$\begin{aligned} Q_1(a,b) &= \int_b^{\infty} xe^{-(x^2+a^2)/2}I_0(ax)\,dx\\ &= e^{-(a^2+b^2)/2}\sum_{k=0}^{\infty}\left(\frac{a}{b}\right)^k I_k(ab), \quad b>a>0,\end{aligned} \tag{18}$$

respectively.

### 4.1. The GML Detector

The probability of choosing signal $\mathbf{s}_l$ over $\mathbf{s}_m$ under $H_m$ is given by

$$P^{GML}(m,l) = \Pr\left(|\mathbf{s}_m^*\mathbf{y}|^2-|\mathbf{s}_l^*\mathbf{y}|^2<0\right).$$

We will begin by stating a general theorem which gives the probability that the difference of two magnitude squared normal random variables is negative.

**Theorem 4.1.** *Let $X$ and $Y$ be complex normal random variables with means $\bar{X}$ and $\bar{Y}$, variances $\sigma_X^2=E[|X-\bar{X}|^2]$ and $\sigma_Y^2=E[|Y-\bar{Y}|^2]$, and cross-covariance $\rho_{XY}=E[(X-\bar{X})(Y-\bar{Y})^*]$. The probability that $|X|^2-|Y|^2<0$ is given by*

$$P = Q_1(a,b)-\frac{\omega_2/\omega_1}{1+\omega_2/\omega_1}I_0(ab)\exp\left[-\frac{1}{2}(a^2+b^2)\right] \tag{19}$$

*where*

$$\begin{aligned} a &= \left[\frac{2\omega_1^2\omega_2(\alpha_1\omega_2-\alpha_2)}{(\omega_1+\omega_2)^2}\right]^{1/2}\\ b &= \left[\frac{2\omega_1\omega_2^2(\alpha_1\omega_1+\alpha_2)}{(\omega_1+\omega_2)^2}\right]^{1/2}\\ \omega_1 &= \sqrt{\tau^2+\frac{1}{\sigma_X^2\sigma_Y^2-|\rho_{XY}|^2}}-\tau\\ \omega_2 &= \sqrt{\tau^2+\frac{1}{\sigma_X^2\sigma_Y^2-|\rho_{XY}|^2}}+\tau\\ \alpha_1 &= \left(|\bar{X}|^2\sigma_Y^2+|\bar{Y}|^2\sigma_X^2-2\mathrm{Re}(\bar{X}^*\bar{Y}\rho_{XY})\right)\\ \alpha_2 &= |\bar{X}|^2-|\bar{Y}|^2\\ \tau &= \frac{\sigma_X^2-\sigma_Y^2}{2\left(\sigma_X^2\sigma_Y^2-|\rho_{XY}|^2\right)},\end{aligned}$$

*and the Marcum Q function $Q_1(a, b)$ and the zeroth-order modified Bessel function are defined in* (18).

**Proof:** See [18, Appendix B]. □

For our problem we have $X = \mathbf{s}_m^* \mathbf{y}$, $Y = \mathbf{s}_l^* \mathbf{y}$, $\bar{X} = \sqrt{E_m}\, e^{j\phi_m}$, $\bar{Y} = \sqrt{E_m}\, e^{j\phi_m} \mathbf{s}_l^* \mathbf{s}_m$, $\sigma_X^2 = \sigma^2$, $\sigma_Y^2 = \sigma^2$, and $\rho_{XY} = \sigma^2 \mathbf{s}_m^* \mathbf{s}_l$. Substituting these values into Theorem 4.1 we obtain the following expression for the pairwise error probability of the GML detector:

$$P^{GML}(m, l) = Q_1\left(\sqrt{\frac{E_m(1 - s_{m,l})}{2\sigma^2}}, \sqrt{\frac{E_m(1 + s_{m,l})}{2\sigma^2}}\right) - \frac{1}{2} \exp\left\{-\frac{E_m}{2\sigma^2}\right\} I_0\left(\frac{E_m |\mathbf{s}_m^* \mathbf{s}_l|}{2\sigma^2}\right), \quad (20)$$

where we have defined $s_{m,l} = \sqrt{1 - |\mathbf{s}_m^* \mathbf{s}_l|^2}$. We can obtain an asymptotic expression for (20) using the results of [19, 20]. Proceeding as in [20] we first write (20) as

$$P(U, V) = Q_1(\sqrt{U - W}, \sqrt{V + W}) - \frac{1}{2} \mathrm{e}^{-U} I_0(V) = \frac{W}{2\pi} \int_0^\pi \frac{\exp(V \cos\phi - U)}{U - V \cos\phi}\, d\phi.$$

where we define

$$U = \frac{E_m}{2\sigma^2}, \quad W = E_m \frac{\mathbf{s}_m^*(\mathbf{I} - \mathbf{s}_l \mathbf{s}_l^*)\mathbf{s}_m}{2\sigma^2 s_{m,l}}, \quad V = \frac{|\mathbf{s}_m^* \mathbf{s}_l| E_m}{2\sigma^2}.$$

This allows us to use the asymptotic expression

$$\lim_{U > |V| \to \infty} P(U, V) = \sqrt{\frac{U + V}{4V}}\, Q(\sqrt{2(U - V)}), \quad (21)$$

where $W = \sqrt{U^2 - V^2}$. Substituting these values into (21) we find that

$$P^{GML}(m, l) \to \sqrt{\frac{1 + |\mathbf{s}_m^* \mathbf{s}_l|}{4|\mathbf{s}_m^* \mathbf{s}_l|}}\, Q\left(\sqrt{\frac{E_m(1 - |\mathbf{s}_m^* \mathbf{s}_l|)}{\sigma^2}}\right). \quad (22)$$

Keeping only the exponential dependency for this expression we find

$$P^{GML}(m, l) \to e^{-\frac{E_m}{2\sigma^2}(1 - |\mathbf{s}_m^* \mathbf{s}_l|)}. \quad (23)$$

*Remark.* In order to obtain an exponential decay of the error probability for the GML detector (with increasing SNR), we require that no two signals be related by a complex scalar. This ensures that each cross-correlation coefficient, $|\mathbf{s}_m^* \mathbf{s}_l|$, is strictly less than one. This means that the signals to be designed must be in at least two complex dimensions.

### 4.2. Error Probability of the Asymptotically Optimal Detector

We now consider the performance of the AO detector introduced in Section 3.2. This analysis is also valid for the optimal detector at large SNRs due to the equivalence of the two detectors (the optimal and the AO) in that regime. We find the pairwise error probability to be

$$P^{AO}(m, l) = \Pr\left(\sqrt{E_l} |\mathbf{y}^* \mathbf{s}_l| - \sqrt{E_m} |\mathbf{y}^* \mathbf{s}_m| > \frac{E_l - E_m}{2}\right). \quad (24)$$

This problem was consider in [16] and [1] and we will simply state that result:

$$\begin{aligned} P^{AO}(m, l) &= \frac{e^{-b}}{a} \int_{y=0}^{\infty} \int_{x=y+\alpha}^{\infty} xy e^{-\eta c y^2 - c x^2} I_0(fxy) \times I_0(gy)\, dx\, dy \\ &= \frac{e^{-b}}{4ac^2} \int_0^\infty w e^{-(\frac{\eta}{2} - \frac{f^2}{8c^2}) w^2} I_0\left(\frac{gw}{\sqrt{2c}}\right) \times Q_1\left(\frac{fw}{2c}, w + \alpha\sqrt{2c}\right) dw, \end{aligned} \quad (25)$$

where

$$\begin{aligned} a &= \frac{\sigma^4 E_m E_l \left(1 - |\mathbf{s}_m^* \mathbf{s}_l|^2\right)}{4}, \\ b &= E_m/\sigma^2, \\ c &= \frac{1}{\sigma^2 E_m E_l \left(1 - |\mathbf{s}_m^* \mathbf{s}_l|^2\right)}, \\ f &= \frac{2|\mathbf{s}_m^* \mathbf{s}_l|}{\sigma^2 \sqrt{E_m E_l}\left(1 - |\mathbf{s}_m^* \mathbf{s}_l|^2\right)}, \\ g &= 2/\sigma^2, \\ \eta &= E_l/E_m, \\ \alpha &= (E_l - E_m)/2. \end{aligned} \quad (26)$$

In the next subsection, we show that at high SNRs, this pairwise error probability approaches the simple form

$$P^{AO}(m,l) \to e^{-\frac{1}{4\sigma^2}(E_m+E_l-2\sqrt{E_m E_l}|\mathbf{s}_m^*\mathbf{s}_l|)}. \quad (27)$$

Notice that when $E_m = E_l$, this simplifies to the exponential bound for the GML detector given in (23), as it must.

*Remark.* In order to ensure that the error probability for the AO detectors decays exponentially, we require that no two signals be related by a phase shift. We can, however, allow pairs of signals to be related by positive scaling (unlike the case of the GML detector). This implies that we can design the signals in one or more complex dimensions.

With these bounds on the error probability, we can consider the problem of designing signals to minimize the appropriate distance measure for use with noncoherent detection. For the general case of unequal energy signaling the appropriate metric is

$$d_{UE}(\{\mathbf{s}_i\}) = \min_{m,l}\left\{E_m + E_l - 2\sqrt{E_m E_l}|\mathbf{s}_m^*\mathbf{s}_l|\right\}. \quad (28)$$

Interestingly, this distance measure can be interpreted as the worst-case Euclidean distance between $\mathbf{s}_m$ and $e^{j\phi}\mathbf{s}_l$ with respect to the phase term, $\phi$. We should point out again that this distance measure is appropriate for the AO detector *and* the optimal detector at large SNRs.

### 4.3. Asymptotic Performance Analysis of the AO Detector

In this section, we prove the result in (27). We are interested in the asymptotic behavior of the pairwise error probability given in (25). In order to get this expression into a tractable form, we will replace some of the terms by asymptotic approximations. We begin by examining the function $Q_1(fw/2c, w+\alpha\sqrt{2c})$. Notice that for a fixed value of $w$, the second parameter is increasing as $\sigma^2$ becomes small, while the first remains constant. Letting $a_1 = fw/2c$ and $b_1 = w+\alpha\sqrt{2c}$, we use the infinite summation form of the Marcum Q-function:

$$Q_1(a_1,b_1) = e^{-\frac{1}{2}(a_1^2+b_1^2)}\sum_{n=0}^{\infty}\left(\frac{a_1}{b_1}\right)^n I_n(a_1b_1), \quad (29)$$

where the $n$th order modified Bessel function, $I_m(z)$, is given by (18). Using the fact that the exponential function is monotonic in its argument we find that for $z>0$,

$$\begin{aligned} I_n(z) = |I_n(z)| &= \frac{1}{2\pi}\left|\int_0^{2\pi} e^{\pm jn\theta}e^{z\cos(\theta)}\,d\theta\right| \\ &\le \frac{1}{2\pi}\int_0^{2\pi} e^{z\cos(\theta)}\,d\theta \\ &\le e^z. \end{aligned} \quad (30)$$

We use this expression together with (29) to find the bounds

$$\begin{aligned} e^{-\frac{1}{2}(a_1^2+b_1^2)}I_o(a_1b_1) &\le Q_1(a_1,b_1) \\ &\le \frac{1}{1-\frac{a_1}{b_1}}e^{-\frac{1}{2}(b_1-a_1)^2}, \end{aligned} \quad (31)$$

where the lower bound is the first term in the sum of (29) and the upper bound follows when we employ our bound on $I_m(a_1b_1)$ and simplify the resulting geometric sum. For large values of $b_1$ we have $I_0(a_1b_1)\to e^{a_1b_1}$, and $a_1/b_1 \to 0$, and consequently

$$Q_1(a_1,b_1) \to e^{-\frac{1}{2}(b_1-a_1)^2} \quad (32)$$

for small values of $\sigma^2$.

Similarly, we replace the function $I_0(\frac{gw}{\sqrt{2c}})$ by $e^{\frac{gw}{\sqrt{2c}}}$ in Eq. (25) since the argument $gw/\sqrt{2c}$ becomes large as $\sigma^2$ vanishes we have the asymptotic approximation

$$P^{AO}(m,l) \to \frac{e^{-b-c\alpha^2}}{4ac^2}\int_0^{\infty} we^{-\beta w^2-\delta w}\,dw, \quad (33)$$

where we have defined

$$\begin{aligned} \beta &= \frac{1}{2}\left(\eta - \frac{f^2}{4c^2} + \left(1-\frac{f}{2c}\right)^2\right) \\ \text{and}\quad \delta &= \left(1-\frac{f}{2c}\right)\alpha\sqrt{2c} - \frac{g}{\sqrt{2c}}. \end{aligned} \quad (34)$$

Applying Eqs. 4.462.2 and 3.462.1 of [21], we find

$$\begin{aligned} &\int_0^{\infty} we^{-\beta w^2-\delta w}\,dw \\ &= \int_{-\infty}^{\infty} we^{-\beta w^2-\delta w}\,dw + \int_0^{\infty} we^{\beta w^2+\delta w}\,dw \\ &= \frac{-\delta\sqrt{\pi}}{2\beta^{3/2}}e^{\frac{\delta^2}{4\beta}} + \frac{1}{2\beta}e^{\frac{\delta^2}{8\beta}}D_{-2}\left(-\frac{\delta}{\sqrt{2\beta}}\right), \end{aligned} \quad (35)$$

where $D_v(x)$ is the *parabolic-cylinder* function of order $v$ [21]. The left-most term in Eq. (35) becomes large as $\sigma^2$ approaches zero, while the right-most term is approaching zero ($|D_{-2}(z)| \ll e^{-z^2/4}$ when $z \gg 1$). Consequently we are left with

$$P^{AO}(m,l) \to \frac{-\delta\sqrt{\pi}}{8\beta^{3/2}ac^2} e^{-b-c\alpha^2+\delta^2/4\beta}. \tag{36}$$

Keeping only the exponential term and expanding the expression we find our final bound:

$$P^{AO}(m,l) \to e^{-\frac{1}{4\sigma^2}(E_m+E_l-2\sqrt{E_m E_l}|\mathbf{s}_m^*\mathbf{s}_l|)}. \tag{37}$$

## 5. Signal Design for the Noncoherent AWGN Channel

In this section we discuss techniques for designing signals for the AWGN which minimize the appropriate metric from the previous section under a strict bandwidth constraint. We will introduce a technique for designing equal energy signals in Section 5.1 and suggest extensions to unequal energy designs in Section 5.2.

### *5.1. Signal Design for Equal Energy Constellations*

In this section we consider designing signals with equal (unit) energy, such that the maximum cross-correlation coefficient is bounded by a constant and the overall bandwidth is constrained. This problem was considered by the authors in [4] and we will describe the results of that paper here and suggest some extensions.

Given the performance measure, $\rho = \max_{l \neq m} |\mathbf{s}_m{}^*\mathbf{s}_l|$, we seek to find the largest cardinality set $\{\mathbf{s}_m\}$ such that $|\mathbf{s}_m^*\mathbf{s}_l|$ is less than $\rho$ for all pairs $l \neq m$. When the absolute bandwidth of the signal constellation is constrained to $B$Hz, the dimensionality of the signal set is correspondingly constrained to $N = BT$ where $T$ is the signaling period [18].

Within this framework we may state the signal design problem as follows: given $N \in \mathbb{N}$ and $0 \leq \rho \leq 1$, find the set $\{\mathbf{s}_m\}_{m=1}^M$ of largest cardinality $M$ satisfying

(1) $\|\mathbf{s}_m\| = 1$ for all $m$
(2) $|\mathbf{s}_m^*\mathbf{s}_l| \leq \rho$ whenever $l \neq m$
(3) $\mathrm{Dim}\{\mathbf{s}_m\} \leq N$.

We see that the signal design problem can also be stated as finding the largest finite subset of the $N$-dimensional complex unit hyper-sphere $\mathcal{SC}_N$, such that every pair of elements has a cross-correlation coefficient of at most $\rho$. Such a set is called a (*complex*) *spherical code*.

We construct the signal set by a method of Successive Updates, whereby a signal, $\mathbf{s}_{K+1}$ is added to $\{\mathbf{s}_k\}_{k=1}^K$. At each iteration we maximize the norm, $\sum_{k=1}^K |\mathbf{s}_k^*\mathbf{s}_{K+1}|^2$, under the constraint that $\max |\mathbf{s}_k^*\mathbf{s}_{K+1}| < \rho$. We initialize our design with two orthogonal signals in $\mathbb{C}^N$ and continue to add signals until the constraints can no longer be met, at which point the dimensionality of the signal set is increased if $N > 2$ or the design is terminated. We continue this process until the dimensionality is equal to $N$ and the constraints can not be met.

To compare our signal designs with OMM for noncoherent detection we consider several different values of the signal dimensionality, $M$, and cross-correlation coefficient, $\rho$. Table 1 lists the achieved cardinalities of our signal design for several values of $M$ along with the Welch bound for each pair $(\rho, M)$ given by [22]

$$N^W = \left\lfloor \min_{\{k: f(k)>0\}} \left\{ f(k) = \frac{1-\rho^{2k}}{\binom{M+k-1}{k}^{-1} - \rho^{2k}} \right\} \right\rfloor, \tag{38}$$

where $\lfloor x \rfloor$ is the largest integer less then the real number, $x$. We see that our designs work well for relatively small signal cardinalities.

To give an example of the performance difference between OMM and NMM, consider the error curves of Fig. 2. We notice that the gap between the two techniques is decreasing as the dimensionality of the signal set is increased, with the NMM designs enjoying twice the spectral efficiency of OMM. This trend becomes more pronounced as the dimensionality is increased,

*Table 1.* Achieved cardinality, $N^A$, versus the Welch bound, $N^W$, for various values of $M$ and $\rho$.

| $\rho$ | $M$ | $N^A$ | $N^W$ |
|---|---|---|---|
| .2 | 12 | 17 | 22 |
| .2 | 14 | 21 | 30 |
| .2 | 16 | 30 | 42 |
| .45 | 4 | 9 | 16 |
| .45 | 5 | 22 | 37 |
| .45 | 6 | 33 | 103 |
| .5 | 2 | 3 | 3 |
| .5 | 3 | 9 | 9 |
| .5 | 4 | 15 | 24 |

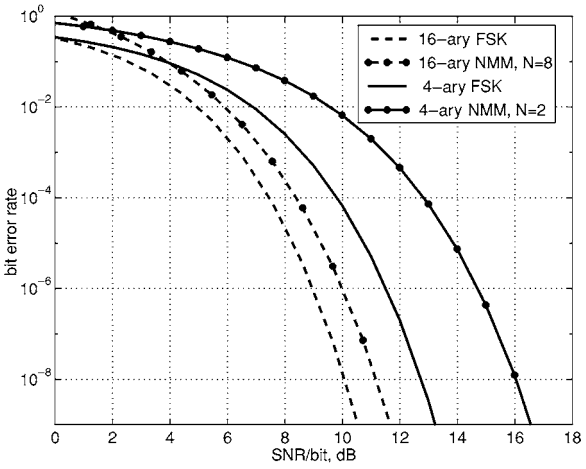


*Figure 2.* Bit error rate versus SNR for several equal-energy OMM and NMM designs.

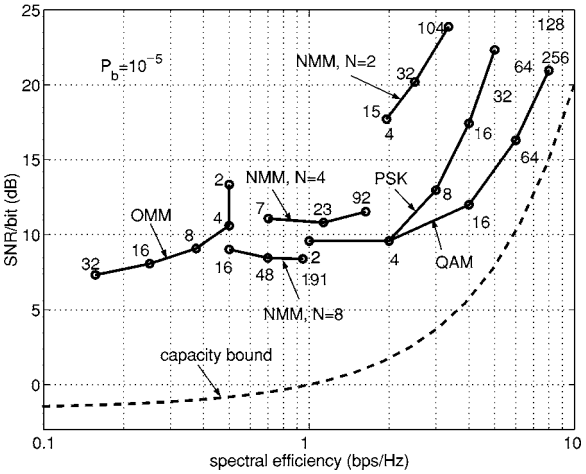


*Figure 3.* Energy and spectral efficiencies of the noncoherent designs.

demonstrating that with a small expenditure in SNR one can obtain a large increase in spectral efficiency relative to OMM.

In Fig. 3 we plot the spectral efficiency $(\log_2(M)/N)$ of our designs versus the energy efficiency (SNR-per-bit required to achieve a probability of bit error of $10^{-5}$). For the NMM designs, we held the dimensionality $N$ fixed and varied the maximum cross-correlation $\rho$. For comparison, we also plot the spectral efficiencies of coherent PAM and QAM modulation as well as the capacity curve for the coherent channel. These results show that we can map out new portions of the energy/spectral efficiency plane through our signal designs, and that NMM can be made more efficient than OMM.

An alternative signal design technique would be to minimize the maximum correlation, $\max |\mathbf{s}_k^* \mathbf{s}_{K+1}|$ without the inequality bounds and continue until this term exceeds $\rho$. In this case we would exchange the inequality constraints of our previous algorithm for an $L_\infty$ optimization functional.

### 5.2. *Signal Design for Unequal Energy Constellations*

On the coherent AWGN channel, it is well known that unequal energy constellations provide a better power-bandwidth trade-off than equi-energy schemes (QAM vs. PSK, for instance) because of the additional degree of freedom. We expect a similar result for the noncoherent channel, where the metric of Eq. (28) is used in the place of Euclidean distance.

We have so far considered a simple trial-and-error procedure in which two shells of equal energy signals, $\mathcal{S}_1 \subset E_1 \mathcal{SC}_N$ and $\mathcal{S}_2 \subset E_2 \mathcal{SC}_N$, are designed; each shell corresponds to a different energy $E_k$. We fixed the cardinality and energy of shell one, $|\mathcal{S}_1|$ and $E_1$, and varied the outer shell energy, $E_2$, and cardinality, $|\mathcal{S}_2|$, so that the worst-case error exponent within the second shell and the worst-case error exponent between the two shells was roughly the same as that of the first shell.

In this manner we constructed a signal set of cardinality $|\mathcal{S}_1| + |\mathcal{S}_2|$ that performed better than an equal-energy signal set of the same cardinality and with the same average energy. In Fig. 4, we plot the probability of symbol error for the two-shell scheme with $|\mathcal{S}_1| = 8$, $|\mathcal{S}_2| = 61$, $E_1 = 1$, and $E_2 = 1.5$. For comparison, we

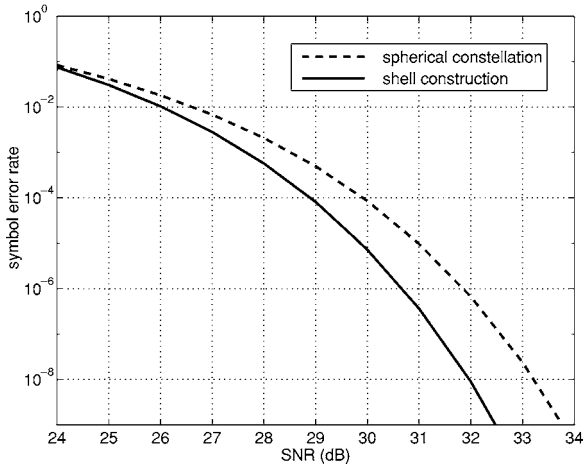


*Figure 4.* Probability of error for the two shell design and a one shell design of the same cardinality.

plot the probability of error for an equal energy constellation of cardinality 69 with the same average energy. We notice that we gain around 1.5 dB in performance over the equal energy scheme through this design.

These results are encouraging, leading us to expect substantial gains over equal energy constellations when systematic design techniques are considered.

## 6. Capacity of Channels with Non-Orthogonal Multipulse Modulation

In order to assess the potential of NMM with coding, we extend the result of [6] for OMM to derive the capacity of the noncoherent channel on which NMM signal sets are employed. The spectral efficiency of the NMM channel is found by normalizing the capacity by the minimum bandwidth required to build the signals. This result is illustrated by evaluating the capacity of NMM signals sets of several cardinalities in two complex dimensions and comparing it with that of binary and quaternary OMM. This demonstrates the improvements in bandwidth efficiency which may be hoped for when employing NMM signaling together with coding.

When the message symbol, $X$, is drawn from an M-ary alphabet we define the capacity of the channel in terms of the sufficient statistic, $\mathbf{y}$, as

$$\begin{aligned} C &= \max_{\mathbf{p}_X} I(X;Y) \\ &= \max_{\mathbf{p}_X} \sum_{m=0}^{M-1} \int_{\mathbf{y}} f(\mathbf{y} \mid X=m)\mathbf{p}_X(m) \\ &\quad \times \log_2 \frac{f(\mathbf{y} \mid X=m)}{f(\mathbf{y})}\, d\mathbf{y} \text{ bits/symbol,} \end{aligned} \tag{39}$$

where $\mathbf{p}_X$ is a probability mass function on $X$ and the integral is taken over the domain of definition for the random variable $\mathbf{y}$ (here $\mathbb{C}^N$).

When the channel is symmetric, as arises when the signals are equi-correlated, the uniform prior distribution, $\mathbf{p}_X(m) = 1/M$ maximizes the mutual information and we have

$$\begin{aligned} C = \log_2 M \Bigg[ 1 - \int_{\mathbf{y}} f(\mathbf{y} \mid X=0) \\ \times \log_M \left( 1 + \sum_{m \neq 0} \frac{f(\mathbf{y} \mid X=m)}{f(\mathbf{y} \mid X=0)} \right) d\mathbf{y} \Bigg] \text{ bits/symbol.} \end{aligned} \tag{40}$$

When the signal constellation does not posses this symmetry, we can still lower bound the capacity through the use of the uniform prior mass to find the mutual information term

$$\begin{aligned} C^* &= \log_2 M \Bigg[ 1 - \frac{1}{M} \sum_{m=0}^{M-1} \int_{\mathbf{y}} f(\mathbf{y} \mid X=m) \\ &\quad \times \log_M \left( 1 + \sum_{l \neq m} \frac{f(\mathbf{y} \mid X=l)}{f(\mathbf{y} \mid X=m)} \right) d\mathbf{y} \Bigg] \text{ bits/symbol.} \end{aligned} \tag{41}$$

Averaging over the uniform phase of the measurement as in (12), we find the conditional likelihood functions to be

$$\begin{aligned} f(\mathbf{y} \mid X=m) = \frac{1}{(\pi\sigma^2)^N} \exp\left\{ -\frac{1}{\sigma^2} \left( \|\mathbf{y}\|^2 + E_m \right) \right\} \\ \times I_0 \left( \frac{2\sqrt{E_m} |\mathbf{y}^* \mathbf{s}_m|}{\sigma^2} \right). \end{aligned} \tag{42}$$

To simplify the presentation let us define the functions

$$\begin{aligned} \Lambda_m(\mathbf{y}) &= 1 + \sum_{l \neq m} \frac{f(\mathbf{y} \mid X=l)}{f(\mathbf{y} \mid X=m)} \text{ and} \\ g_m(\mathbf{z}) &= \exp\left\{ -\frac{1}{\sigma^2} 2\sqrt{E_m}\, \mathrm{Re}(\mathbf{z}^* \mathbf{s}_m) \right\} \\ &\quad \times I_o \left( \frac{2\sqrt{E_m} |\mathbf{z}^* \mathbf{s}_m|}{\sigma^2} \right) \log_M(\Lambda_m(\mathbf{z})). \end{aligned} \tag{43}$$

Then placing the conditional multivariate normal distribution on $\mathbf{z}$,

$$f(\mathbf{z} \mid X=m) = \frac{1}{(\pi\sigma^2)^N} \exp\left\{ -\frac{1}{\sigma^2} \|\mathbf{z} - \sqrt{E_m}\, \mathbf{s}_m\|^2 \right\}, \tag{44}$$

we find the following formulation for the NMM capacity:

$$C^* = \log_2 M \left[ 1 - \frac{1}{M} \sum_{m=0}^{M-1} E_{\mathbf{z}|X=m}\{ g_m(\mathbf{z}) \} \right]. \tag{45}$$

When the constellation is symmetric we find

$$C = \log_2 M [1 - E_{\mathbf{z}|X=0}\{ g_o(\mathbf{z}) \}]. \tag{46}$$

The advantage of this formulation is that Monte-Carlo integration techniques may be employed to numerically

determine the channel capacity, even when the multidimensional integrals in equations (40) and (41) are infeasible due to large values of $N$. This is a multi-dimensional generalization of the methods of Ungerboeck [23], which were developed for the coherent channel.

### 6.1. *Examples*

To quantify the bandwidth efficiencies of the various signal constellations with coding, we define the coded spectral efficiency, SE, to be the channel capacity divided by the minimum bandwidth needed to build the signals. For NMM signals with a $N$ dimensional basis, the spectral efficiency is given in bits/second/Hertz by

$$SE^* = \frac{C^*}{N} \text{ bps/Hz}, \tag{47}$$

with $N = M$ for OMM.

In Fig. 5 we plot the spectral efficiencies of several different sized NMM constellations in two dimensions as well as binary and 4-ary OMM for the AWGN channel. Notice that the 4-ary NMM signal design achieves twice the efficiency of the OMM designs, enjoying the bandwidth of binary OMM with the asymptotic rate of 4-ary OMM. For comparison, we plot the spectral efficiencies of coherent quadriphase shift keying(QPSK) together with that of a 16-ary NMM design (in two dimensions). The capacity of the QPSK channel was computed as in [23].

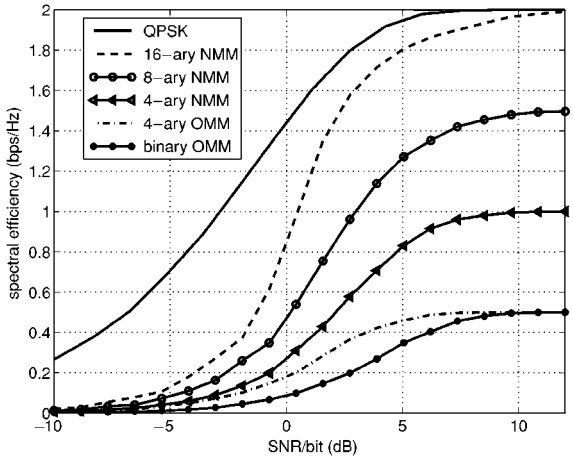


*Figure 5.* Spectral efficiencies for noncoherent, coded, OMM and NMM versus the channel SNR per bit on the AWGN channel. In each case the NMM signals were constructed in a two dimensional basis. The spectral efficiency of coherent QPSK as derived in [23] is plotted for comparison.

## 7. Convolutional Coding on the Noncoherent AWGN Channel

Several low rate convolutional codes for use with OMM were presented in [7]. The rate $R = 1/Q$ convolutional encoder produces a $Q$-length sequence of $M$-ary output symbols for each q-ary input symbol with constraint length $K$ (i.e., each output symbol is a function of the $K$ most recent input symbols). We may view the codes as a mapping with memory, from $GF(q)$, the Galois field of cardinality $q$, to $GF(M)^Q$, with $GF(q)$ taken to be a sub-field of $GF(M)$. This vector of symbols is then read out in serial and each symbol is mapped to a continuous time waveform by associating the $i$th member of a set of $M$ waveforms to the output symbol $i \in GF(M)$. The time series of output vectors are related to the input sequence, $u_p$, by the convolutional mapping

$$\mathbf{f}_j = \sum_{k=0}^{K-1} \mathbf{g}_k u_{j-k}, \tag{48}$$

where each $\mathbf{g}_k$ is a $1 \times Q$ vector with each element lying in $GF(M)$ and all arithmetic is done in $GF(M)$.

At the decoder a sequence of measurements, $\{\mathbf{y}_n(l)\}$, is received with $\mathbf{y}_n(l)$ corresponding to the $l$th entry in the $n$th transmitted code sequence, $\mathbf{c} = [\mathbf{f}_1\, \mathbf{f}_2 \cdots]$,

$$\mathbf{y}_t = \sqrt{E_{c_t}}\, e^{j\phi_t} \mathbf{s}_{c_t} + \mathbf{n}(t), \tag{49}$$

where $E_{c_t}$ is the energy of the $c_t$th code symbol and $t = nQ + l$, i.e. $c_t = \mathbf{f}_n(l)$. We consider asymptotically optimal decoding with decisions

$$\hat{k} = \arg\max_k \sum_{t=0}^{PQ-1} -E_{c_t} + 2\sqrt{E_{c_t}} \left| \mathbf{y}_t^* \mathbf{s}_{c_t^k} \right|, \tag{50}$$

where $\{\mathbf{c}^k\}$ is the set of allowable code sequences and we have assumed that each sequence is composed of $P$ length-Q blocks. For the special case of equal energy code symbols ($E_{c_t}$ is constant) we have the square law decoder:

$$\hat{k} = \arg\max_k \sum_{t=0}^{PQ-1} \left| \mathbf{y}_t^* \mathbf{s}_{c_t^k} \right|^2. \tag{51}$$

This decoding can be performed in the usual way via a maximum likelihood trellis search, typically with the Viterbi algorithm. The metric for a branch which leaves state $p$ at time $n$ and enters state $j$ at time $n+1$ is given by

$$B_{p,j} = \begin{cases} \displaystyle\sum_{t=nQ}^{(n+1)Q-1} -E_{c_t} + 2\sqrt{E_{c_t}}\left|\mathbf{y}_t^* \mathbf{s}_{c_t^{pj}}\right|, \\ \qquad \text{unequal codeword energies} \\ \displaystyle\sum_{t=nQ}^{(n+1)Q-1} \left|\mathbf{y}_t^* \mathbf{s}_{c_t^{pj}}\right|^2, \\ \qquad \text{equal codeword energies} \end{cases}, \tag{52}$$

where $c_t^{pj}$ is the $t$th code symbol corresponding to the $Q$-length codeword associated with the transition from state $p$ to state $j$. The survivor path metric at state $j$ and at time $n$ is given by

$$\lambda_n(j) = \max_{p \in \mathcal{S}_j} \{\lambda_{n-1}(p) + B_{p,j}\}, \tag{53}$$

where $\mathcal{S}_j$ is the set of states which can transition to state $j$ in one step.

A block diagram of the encoder is shown in Fig. 6, where we assume that each transmit sequence ends with an all zero sequence to terminate the trellis.

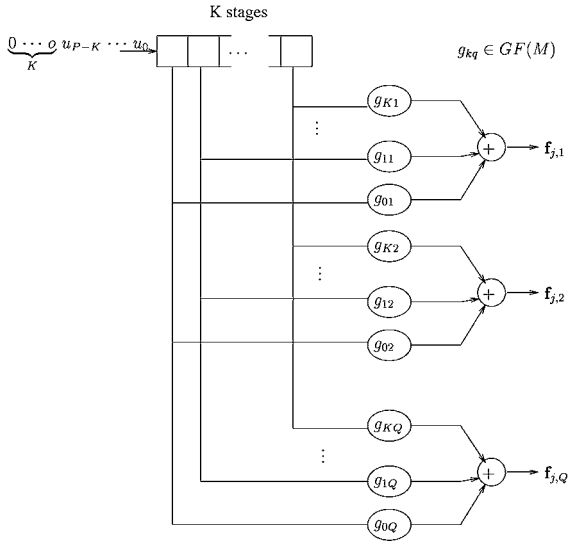


*Figure 6.* Block diagram of the convolutional encoder.

The authors of [7] developed several codes for $q = 2$ (binary to M-ary) and $q = M$ (M-ary to M-ary) which are optimal with respect to the information spectrum (they actually used a truncated spectrum, keeping the first four terms). That is, they have the largest possible free distance, $d_{free}$, and the optimal distribution of information symbols, $N_S(w)$, associated with remergent trellis paths of Hamming weight $w$ for $d_{free} \leq w \leq d_{free} + 3$. They considered performance on the OMM channel. In light of our development of complex spherical codes, we can extend the results of [7] by replacing the orthogonal waveforms in their development by $M$ correlated waveforms in a low dimensional, $N \leq M$, subspace. This allows us to increase the bandwidth of the convolutionally coded systems of [7] by a factor of $M/N$. It is of interest to obtain a simple characterization of the increase in SNR/bit needed to obtain the same performance with OMM and the spectrally more efficient NMM scheme.

We assume that the signals have equal cross-correlation, $|\rho|$, and equal energies, $E_c$. This appears to be well justified from our numerical simulations and even when this is not true, the corresponding expressions act as an upper bound whenever $|\mathbf{s}_m^* \mathbf{s}_l| \leq |\rho|$ for all $m$ and $l$. Proceeding as in [7], we employ the transfer function bound on the bit error probability

$$P_b < \frac{2^{k-1}}{2^k - 1} \sum_{w=d_{free}}^{\infty} N_s(w) P_2(w), \tag{54}$$

where $k = 1$ for binary-to-M-ary codes and $k = \log_2(M)$ for the M-ary codes and $N_s(w)$ is the number of detours from the all-zero code sequence with Hamming weight $w$. The two codeword error probabilities, $P_2(w)$ with Hamming distance $w$ are derived below for the AWGN channel.

Let $\mathbf{c}^1$ and $\mathbf{c}^2$ be two code sequences which differ in the $w$ positions $t_1, \ldots, t_w$. Assuming that codeword $\mathbf{c}^1$ was transmitted, the decoder chooses $\mathbf{c}^2$ over $\mathbf{c}^1$ whenever

$$\sum_{i=1}^{w} \left|\mathbf{y}_{t_i}^* \mathbf{s}_{c_{t_i}^1}\right|^2 - \left|\mathbf{y}_{t_i}^* \mathbf{s}_{c_{t_i}^2}\right|^2 < 0, \tag{55}$$

where $\mathbf{s}_{c_{t_i}^k}$ is the symbol corresponding to the $t_i$th position of the codeword $\mathbf{c}^k$. The following theorem (a generalization of Theorem 4.1) gives the probability of error for the difference of quadratic forms which obey this general model.

**Theorem 7.1.** *Let the quadratic form $D$ be given by*

$$D = \sum_{i=1}^{w} \left( |X_i|^2 - |Y_i|^2 \right) \tag{56}$$

*where the pairs $(X_i, Y_i)$ are mutual statistically independent complex normal random variables with means $\bar{X}_i$ and $\bar{Y}_i$, variances $E[|X_i - \bar{X}_i|^2] = \sigma_X^2$ and $E[|Y_i - \bar{Y}_i|^2] = \sigma_Y^2$, and equal magnitude cross-correlations, $|E[(X_i - \bar{X}_i)(Y_i - \bar{Y}_i)^*]| = |\rho_{XY}|$. Then the probability that $D < 0$ is given by*

$$\begin{aligned}
&\text{Prob}(D < 0) \\
&= Q_1(a,b) - I_0(ab) \exp\left[ -\frac{1}{2}(a^2 + b^2) \right] \\
&\quad + \frac{I_0(ab) \exp\left[ -\frac{1}{2}(a^2 + b^2) \right]}{(1 + \omega_2/\omega_1)^{2w-1}} \sum_{i=0}^{w-1} \binom{2w-1}{i} \left( \frac{\omega_2}{\omega_1} \right)^i \\
&\quad + \frac{\exp\left[ -\frac{1}{2}(a^2 + b^2) \right]}{(1 + \omega_2/\omega_1)^{2w-1}} \sum_{n=1}^{w-1} I_n(ab) \sum_{i=0}^{w-1-n} \binom{2w-1}{i} \\
&\quad \times \left[ \left( \frac{b}{a} \right)^n \left( \frac{\omega_2}{\omega_1} \right)^i - \left( \frac{a}{b} \right)^n \left( \frac{\omega_2}{\omega_1} \right)^{2w-1-i} \right],
\end{aligned}$$

*where*

$$\begin{aligned}
a &= \left[ \frac{2\omega_1^2 \omega_2 (\alpha_1 \omega_2 - \alpha_2)}{(\omega_1 + \omega_2)^2} \right]^{1/2} \\
b &= \left[ \frac{2\omega_1 \omega_2^2 (\alpha_1 \omega_1 + \alpha_2)}{(\omega_1 + \omega_2)^2} \right]^{1/2} \\
\omega_1 &= \sqrt{\tau^2 + \frac{1}{\sigma_X^2 \sigma_Y^2 - |\rho_{XY}|^2}} - \tau \\
\omega_2 &= \sqrt{\tau^2 + \frac{1}{\sigma_X^2 \sigma_Y^2 - |\rho_{XY}|^2}} + \tau \\
\alpha_1 &= \sum_{i=1}^{w} \left( |\bar{X}_i|^2 \sigma_Y^2 + |\bar{Y}_i|^2 \sigma_X^2 - 2\text{Re}(\bar{X}_i^* \bar{Y}_i \rho_{XY}) \right) \\
\alpha_2 &= \sum_{i=1}^{w} |\bar{X}_i|^2 - |\bar{Y}_i|^2 \\
\tau &= \frac{\sigma_X^2 - \sigma_Y^2}{2\left( \sigma_X^2 \sigma_Y^2 - |\rho_{XY}|^2 \right)}
\end{aligned}$$

**Proof:** See [18, Appendix B]. □

For our problem we have $X_i = \mathbf{y}_{t_i}^* \mathbf{s}_{c_{t_i}^1}$, $Y_i = \mathbf{y}_{t_i}^* \mathbf{s}_{c_{t_i}^2}$, $\bar{X}_i = \sqrt{E_c}\, e^{j\phi_{t_i}}$, $\bar{Y}_i = \sqrt{E_c}\, e^{j\phi_{t_i}} \mathbf{s}_{c_{t_i}^1}^* \mathbf{s}_{c_{t_i}^2}$, $\sigma_X^2 = \sigma^2$, $\sigma_Y^2 = \sigma^2$, and $|\rho_{XY}| = \sigma^2 |\mathbf{s}_{c_{t_i}^1}^* \mathbf{s}_{c_{t_i}^2}| = \sigma^2 |\rho|$. Employing Theorem 7.1 with these values we find

$$\begin{aligned}
P_2(w) &= Q_1\left( \sqrt{\frac{E_c w(1-s)}{2\sigma^2}}, \sqrt{\frac{E_c w(1+s)}{2\sigma^2}} \right) \\
&\quad - I_0\left( \frac{w|\rho|}{2\sigma^2} \right) \exp\left( -\frac{w}{2\sigma^2} \right) \\
&\quad \times \left\{ 1 - \frac{1}{2^{2w-1}} \sum_{p=1}^{w-1} \binom{2w-1}{p} \right\} \\
&\quad + \frac{\exp\left( -\frac{E_c w}{2\sigma^2} \right)}{2^{2w-1}} \sum_{n=1}^{w-1} I_n\left( \frac{E_c w |\rho|}{2\sigma^2} \right) \\
&\quad \times \frac{(1+s)^n - (1-s)^n}{|\rho|^n} \sum_{p=1}^{w-1-n} \binom{2w-1}{p},
\end{aligned} \tag{57}$$

where $s = \sqrt{1 - |\rho|^2}$. The term $E_c/\sigma^2$ is the *coded* signal-to-noise ratio, $E_c/\sigma^2 = (k/Q) E_S/\sigma^2$ where $E_S$ is the *uncoded* energy per symbol and $k$ is defined as in (54).

**Theorem 7.2.** *Let the error probability associated with a quadratic form becoming negative be of the form*

$$\begin{aligned}
P &= Q_1(a,b) - I_0(ab) \exp\left[ -\frac{1}{2}(a^2 + b^2) \right] \\
&\quad + \frac{I_0(ab) \exp\left[ -\frac{1}{2}(a^2 + b^2) \right]}{(1 + \omega_2/\omega_1)^{2w-1}} \sum_{i=0}^{w-1} \binom{2w-1}{i} \\
&\quad \times \left( \frac{\omega_2}{\omega_1} \right)^i + \frac{\exp\left[ -\frac{1}{2}(a^2 + b^2) \right]}{(1 + \omega_2/\omega_1)^{2w-1}} \\
&\quad \times \sum_{n=1}^{w-1} I_n(ab) \sum_{i=0}^{w-1-n} \binom{2w-1}{i} \\
&\quad \times \left[ \left( \frac{b}{a} \right)^n \left( \frac{\omega_2}{\omega_1} \right)^i - \left( \frac{a}{b} \right)^n \left( \frac{\omega_2}{\omega_1} \right)^{2w-1-i} \right],
\end{aligned} \tag{58}$$

*where $a$, $b$, $\omega_1$, and $\omega_2$ are defined as in Theorem 7.1. Then under the assumption that $b \gg a$ as the SNR grows large, we find that the probability approached the exponential form*

$$P = e^{-1/2(a-b)^2}. \tag{59}$$

**Proof:** We employ the asymptotic relations

$$\begin{aligned}
&Q_1(a,b) \to e^{-1/2(a-b)^2} \quad \text{and} \\
&e^{-1/2(a^2+b^2)} I_n(ab) \to e^{-1/2(a-b)^2}
\end{aligned} \tag{60}$$

as $a$ and $b$ grow large, where we have kept only the exponential dependencies of the functions using (see e.g. [17, 24]):

$$Q_1(a,b) \approx Q(b-a) \quad (b \gg 1, b \gg b-a)$$
$$I_n(x) = \frac{e^x}{\sqrt{2\pi x}}\left[1 + O\left(\frac{1}{x}\right)\right]. \tag{61}$$

Here $Q(x)$ denotes the standard normal cumulative function

$$Q(x) = \frac{1}{\sqrt{2\pi}} \int_x^\infty e^{-z^2/2}\, dz, \tag{62}$$

which has the asymptotic dependency

$$Q(x) \to e^{-\frac{x^2}{2}}, \tag{63}$$

keeping only the exponential term. When these expressions are substituted into (58) and the exponential dependency is isolated, the theorem follows. □

With the help of Theorem 7.2 we find that at large SNRs the two-codeword error probabilities approach

$$P_2(w) \to e^{-\frac{E_c w}{2\sigma^2}(1-|\rho|)}. \tag{64}$$

The corresponding transfer function bound of (54) approaches the form

$$\frac{2^{k-1}}{2^k - 1} \sum_{w=d_{free}}^{\infty} N_s(w) P_2(w) \to \sum_{w=d_{free}}^{\infty} N_s(w) e^{-\frac{E_c w}{2\sigma^2}(1-|\rho|)}$$
$$\to e^{-\frac{E_c d_{free}}{2\sigma^2}(1-|\rho|)}, \tag{65}$$

keeping only the dominant exponent. This result demonstrates the importance of the free distance in designing convolutional codes for use with NMM modulation, at least asymptotically.

### *7.1. Numerical Results*

In Fig. 7 we show the spectral efficiencies, $SE = R\log_2(M)/N$, and energy efficiencies, $E_S/\sigma^2$ ($E_S = Q/kE_c$ is the uncoded symbol energy), of the M = 16-ary convolutional codes of [7] of rates $R = 1/2$ and $R = 1/3$ for various values of the dimensionality $N$. The constraint length is $K = 3$ for each code and the generator matrices are given by

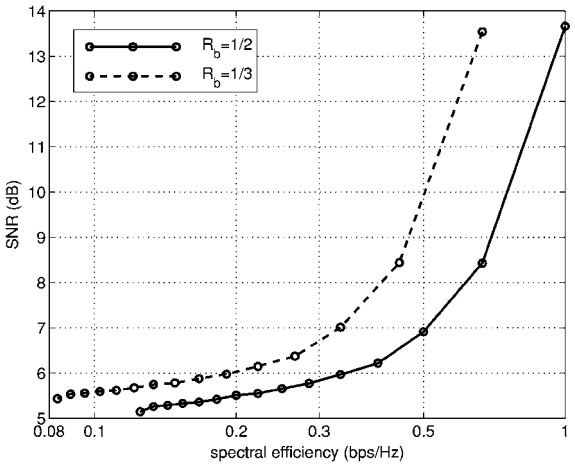


*Figure 7.* Energy and spectral efficiencies of the noncoherent designs on the AWGN channel with coding on a 16-ary alphabet.

$$\mathbf{G}_{1/2} = \begin{bmatrix} 1 & 1 & \alpha^4 \\ 1 & \alpha & \alpha^4 \end{bmatrix} \qquad \mathbf{G}_{1/3} = \begin{bmatrix} 1 & 1 & \alpha^4 \\ 1 & \alpha & \alpha^4 \\ 1 & \alpha^2 & \alpha^9 \end{bmatrix}, \tag{66}$$

where $\alpha$ is a root of $x^4 + x + 1$ in GF(16). The signal constellations were designed as in Section 5.1 with the smallest value of $|\rho|$ needed to achieve the desired cardinality ($M = 16$ for these examples) employed for each value of $N$. The energy efficiencies were calculated via Eq. (54) with $P_b$ fixed at $10^{-5}$ and are hence conservative. A key attribute of these plots is that it is possible to increase the spectral efficiency of these codes significantly with a small loss in the energy efficiency. The potential gains grow with dimensionality as the required cross-correlation $\rho$ grows small "quickly" as the cardinality increases. We also notice that the codes which were designed for OMM are also good for NMM. The signal design problem does not change when coding is introduced, which justifies the use of signals designed in the context of uncoded NMM.

## 8. Extensions to the Rayleigh Fading Channel

In this section we outline the extensions to noncoherent communication on the single-antenna Rayleigh fading channel. In wireless communication the channel often has a randomly time-varying impulse response due to atmospheric effects. This can also be caused by the motion of the transmitter and/or receiver in a mobile

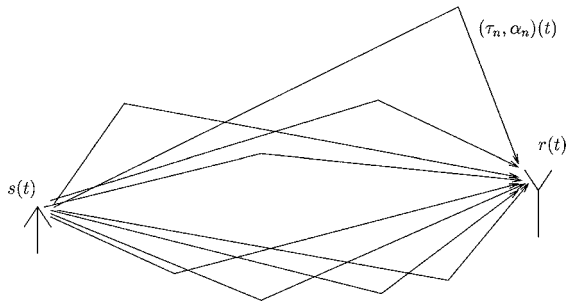


*Figure 8.* The fading multipath channel.

system in which the physical surroundings of the communicator are varying. A useful model for such effects is the *multipath* fading channel, wherein the transmission of the signal $s(t)$ results in the reception of the signal

$$x(t) = \sum_{n=1}^{N} \alpha_n(t) s(t - \tau_n(t)). \tag{67}$$

In general the path parameters $\alpha_n(t)$ and $\tau_n(t)$ are randomly time-varying. This process is shown in Fig. 8. For ionospheric or tropospheric propagation we have $N \gg 1$ and we invoke the Central Limit Theorem [25] to simplify our model to

$$r(t) = \alpha(t) s(t) + n(t), \tag{68}$$

where $\alpha(t)$ is a complex normal random variable for each $t$. We have assumed that the time delays, $\tau_n(t)$, are small relative to the support of the signal so that $s(t - \tau_n(t)) \approx s(t)$.

We will assume that the time-varying fading process is constant in one signaling interval but can change significantly over a few intervals. This leads to the following model for the received signal:

$$r(t) = \alpha s(t) + n(t), \quad 0 \le t < T. \tag{69}$$

The fading amplitude, $\alpha$, is a complex normal random variable with power $E[|\alpha|^2] = \gamma$.

We assume that the signals have equal energy normalized to $\|\mathbf{s}_m\| = 1$ for each $m$, the symbol energy is absorbed into the fading parameter $\alpha$. Conditioned on the transmission of signal $\mathbf{s}_m$, the vector $\mathbf{y}$ is distributed as a complex normal random vector with mean zero and correlation matrix

$$\mathbf{R}_{\mathbf{yy}}^{m} = E[\mathbf{y}\mathbf{y}^*] = \gamma \mathbf{s}_m \mathbf{s}_m^* + \sigma^2 \mathbf{I}. \tag{70}$$

The measurement has the likelihood function

$$f(\mathbf{y} \mid X = m) = \frac{1}{\pi^N \left|\mathbf{R}_{\mathbf{yy}}^{m}\right|} e^{-\mathbf{y}^* (\mathbf{R}_{\mathbf{yy}}^{m})^{-1} \mathbf{y}}, \tag{71}$$

and the maximum likelihood detector (assuming equal prior probabilities) is

$$\hat{m} = \arg\min_m \mathbf{y}^* \left(\mathbf{R}_{\mathbf{yy}}^{m}\right)^{-1} \mathbf{y} \tag{72}$$

$$= \arg\max_m |\mathbf{s}_m^* \mathbf{y}|^2 . \tag{73}$$

The pairwise probability of error of the above square law detector is given by

$$P(m, l) = \Pr\left(|\mathbf{s}_m^* \mathbf{y}|^2 - |\mathbf{s}_l^* \mathbf{y}|^2 < 0\right). \tag{74}$$

To analyze this error probability we may use Theorem 4.1 with $X = \mathbf{s}_m^* \mathbf{y}$, $Y = \mathbf{s}_l^* \mathbf{y}$, $\bar{X} = 0$, $\bar{Y} = 0$, $\sigma_X^2 = \gamma + \sigma^2$, $\sigma_Y^2 = \gamma |\mathbf{s}_m^* \mathbf{s}_l|^2 + \sigma^2$, and $\rho_{XY} = \gamma \mathbf{s}_m^* \mathbf{s}_l + \sigma^2 \mathbf{s}_m^* \mathbf{s}_l$. Since $Q_1(0, 0) = 1$ and $I_0(0) = 1$ we find that

$$P(m, l) = \frac{1}{1 + \frac{\omega_2}{\omega_1}}, \tag{75}$$

where

$$\omega_1 = \frac{\sqrt{\gamma^2 s_{ml}^2 + 4\sigma^2(\sigma^2 + \gamma)} - \gamma s_{ml}}{2\sigma^2(\sigma^2 + \gamma) s_{ml}}$$

$$\omega_2 = \frac{\sqrt{\gamma^2 s_{ml}^2 + 4\sigma^2(\sigma^2 + \gamma)} + \gamma s_{ml}}{2\sigma^2(\sigma^2 + \gamma) s_{ml}} \tag{76}$$

where $s_{ml} = \sqrt{1 - |\mathbf{s}_m^* \mathbf{s}_l|^2}$.

Notice that $s_{m,l} = 1$ for orthogonal signals, and the corresponding error probability is simply

$$P(m, l) = \frac{1}{2 + \frac{\gamma}{\sigma^2}}, \tag{77}$$

which is the usual probability of error for binary orthogonal signaling on the Rayleigh fading channel (see e.g. [18]).

To determine the asymptotic behavior of the error probability for the general NMM case, we will expand the square root terms which appear in $\omega_1$ and $\omega_2$ in a Taylor series around $\sigma^2 = 0$ to find

$$\sqrt{\gamma^2 s_{ml}^2 + 4\sigma^2(\sigma^2 + \gamma)} \approx \sqrt{\gamma^2 s_{ml}^2 + 4\gamma\sigma^2}$$

$$\approx \gamma s_{ml} + \frac{2\sigma^2}{s_{ml}}. \tag{78}$$

Substituting the resulting expressions into (75) we find

$$P(m,l) \to \frac{1}{2+\frac{\gamma s_{ml}^2}{\sigma^2}}, \tag{79}$$

which has the same form as the error probability for orthogonal signaling with the SNR modified by the cross-correlation factor $s_{ml}^2$.

Since the probability of error depends only the cross-correlation between the signals we may employ the successive updates algorithm developed in Section 5 to design signals for the Raleigh channel without modification.

### 8.1. *Capacity of the Rayleigh Fading NMM Channel*

We proceed exactly as we did for the AWGN channel. With the likelihood function specified in (71), and defining $\Lambda_m(\mathbf{y})$ as in (43), we find

$$C^* = \log_2 M\left[1 - \frac{1}{M}\sum_{m=0}^{M-1} E_{\mathbf{y}|X=m}\{\log_M(\Lambda_M(\mathbf{y}))\}\right]. \tag{80}$$

### 8.2. *Examples*

We plot the spectral efficiency curve for the 4-ary NMM signal design together with those of binary and 4-ary OMM for the Rayleigh fading channel in Fig. 9. Notice that we see a dramatic improvement for the correlated signal design over the orthogonal designs, exactly as we saw on the AWGN channel in Section 6.

### 8.3. *Convolutional Coding on the Rayleigh Fading Channel*

We may use the coding techniques developed in Section 7 for the Rayleigh channel. We assume that the coded data is interleaved prior to transmission and deinterleaved before decoding so that the fading may be considered independent from symbol to symbol. With this assumption, the only difference from the AWGN channel is the error analysis. We will further assume that the signals have equal cross-correlation magnitude, $|\mathbf{s}_m^*\mathbf{s}_l| = |\rho|$.

When square-law detection is performed on the Rayleigh fading channel we again label the positions

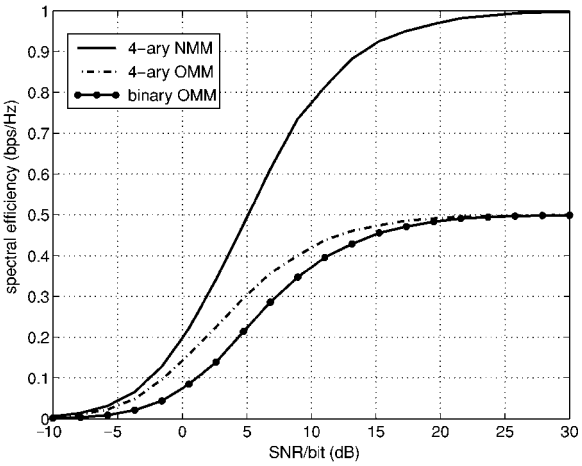


*Figure 9.* Spectral Efficiencies for noncoherent, coded, OMM and NMM versus the channel SNR per bit for the Rayleigh fading channel. The NMM signals were constructed in a two dimensional basis.

in which the codewords differ by $t_1, \ldots, t_w$. We choose $\mathbf{c}^2$ over $\mathbf{c}^1$ whenever $\Gamma = \sum |\mathbf{y}_{t_i}^* \mathbf{s}_{c_{t_i}^1}|^2 - |\mathbf{y}_{t_i}^* \mathbf{s}_{c_{t_i}^1}|^2 < 0$.

To find the error probability, we may use Theorem 7.1 with $X_i = \mathbf{y}_{t_i}^* \mathbf{s}_{c_{t_i}^1}$, $Y_i = \mathbf{y}_{t_i}^* \mathbf{s}_{c_{t_i}^1}$, $\bar{X} = 0$, $\bar{Y} = 0$, $\sigma_X^2 = \gamma_c + \sigma^2$, $\sigma_Y^2 = \gamma_c|\rho|^2 + \sigma^2$, and $|\rho_{XY}| = \gamma_c|\rho| + \sigma^2|\rho|$, where $\gamma_c$ is the average energy in the coded symbol. Since $Q_1(0,0) = 1$, $I_0(0) = 1$, and $I_n(0) = 0$ for $n > 1$ we find that

$$P_2(w) = \frac{1}{\left(1+\frac{\omega_2}{\omega_1}\right)^{2w-1}} \sum_{k=1}^{w-1} \binom{2w-1}{k} \left(\frac{\omega_2}{\omega_1}\right)^k, \tag{81}$$

where

$$\omega_1 = \frac{\sqrt{\gamma^2 s^2 + 4\sigma^2(\sigma^2+\gamma)} - \gamma s}{2\sigma^2(\sigma^2+\gamma)s}$$
$$\omega_2 = \frac{\sqrt{\gamma^2 s^2 + 4\sigma^2(\sigma^2+\gamma)} + \gamma s}{2\sigma^2(\sigma^2+\gamma)s} \tag{82}$$

and $s = \sqrt{1-|\rho|^2}$.

To gain insight into this expression we consider the behavior of the error probability at large SNRs. We may use the Taylor series expansion of $\omega_1$ and $\omega_2$ from (78) to find that $\omega_2/\omega_1 \to 1 + \gamma_c s^2/\sigma^2$. Letting $\xi = \sigma^2/(\gamma_c s)$ denote the reciprocal coded SNR we have

$$P_2(w) = \sum_{k=1}^{w-1} \binom{2w-1}{k} \frac{\xi^{2w-1-k}}{(1+\xi)^{2w-1}} \tag{83}$$

$$\to \sum_{k=1}^{w-1} \binom{2w-1}{k} \xi^{2w-1-k} \tag{84}$$

$$= \binom{2w-1}{w-1} \xi^{w} + \binom{2w-1}{w-2} \xi^{w+1} + \cdots + \binom{2w-1}{1} \xi^{2w-2}. \tag{85}$$

The error probability approaches a polynomial in the reciprocal SNR, $\xi$, with leading coefficient of order $w$. Similarly, the transfer function bound of (54) approaches the form

$$\frac{2^{k-1}}{2^k-1} \sum_{w=d_{free}}^{\infty} N_s(w) P_2(w) \to \frac{2^{k-1}}{2^k-1} \sum_{w=d_{free}}^{\infty} N_s(w) \sum_{k=1}^{w-1} \binom{2w-1}{k} \xi^{2w-1-k}, \tag{86}$$

which is a polynomial with leading coefficient of order $w = d_{free}$. We therefore refer to $d_{free}$ as the *diversity order* of the convolutional code. Notice that diversity is often achieved through either spatial separation of sensors or frequency division multiplexing (see e.g. [18]) while here we employ code-diversity to combat the Rayleigh fading channel.

***8.3.1. Numerical Results.*** In Fig. 10 we plot the spectral and energy efficiencies of the 16-ary convolutional codes employed in Section VII-A on the Rayleigh fading channel. We notice that the curves have the same general shape as observed for the AWGN channel in Fig. 7, demonstrating that we may effectively trade energy efficiency for spectral efficiency. Notice also that the performance loss due to the fading is substantial when compared with the AWGN channel. This motivates the extension of the results to multiple transmit and receive antennas, work which has been carried out in [9].

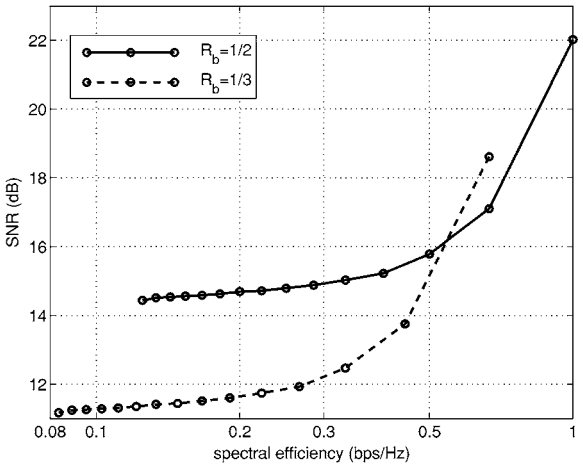


*Figure 10.* Energy and spectral efficiencies of the noncoherent designs on the Rayleigh fading channel with coding on a 16-ary alphabet.

## 9. Equalization

We now consider the problem of noncoherent signaling over a dispersive channel. We will assume that the channel response has been determined and develop a zero-forcing equalizer to combat the ensuing inter-symbol interference. These results were originally developed for the invertible channel in [3] and were extended to the non-invertible channel in [12, 13].

### *9.1. MIMO System Model*

In this section we develop a multiple-input multiple output (MIMO) model for the ISI channel with NMM signaling. We consider communication over a bandpass channel on which the user transmits one of M waveforms every $T$ seconds corresponding to one of $M$ possible information symbols. The waveforms then pass through a channel to yield the composite normalized low-pass equivalent waveforms, $\{s_m(t-kT)\}$, corresponding to the symbols transmitted at time index $k$. We obtain the following low-pass equivalent model for the ISI channel:

$$r(t) = \sum_{k=-\infty}^{\infty} A_{l_k}(k) s_{l_k}(t-kT) + n(t), \tag{87}$$

where $A_{l_k} = \sqrt{E_{l_k}}\, e^{j\phi_{l_k}}$ is the complex amplitude associated with the passband composite waveform for the $l_k$th signal in the $k$th signaling interval, and $N(t)$ is a complex white Gaussian noise process with power $\sigma^2$.

To form a set of sufficient statistics for the detection problem we match the received signal, $r(t)$, against each of the possible transmitted signals $s_m(t-kT)$ to form the matched filter outputs

$$y_m(n) = \int_{-\infty}^{\infty} r(t) \overline{s_m}(t-nT)\, dt. \tag{88}$$

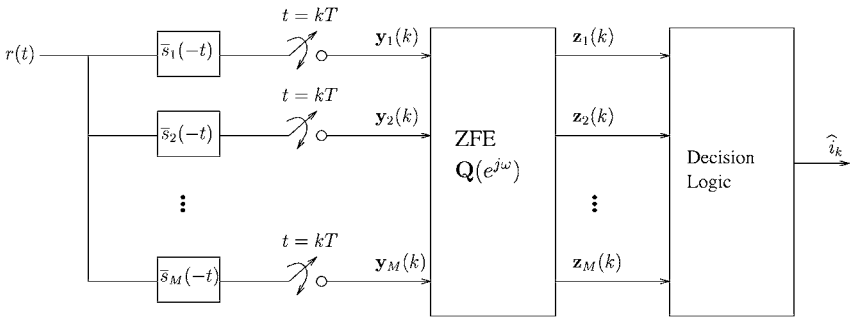


*Figure 11.* Matched filter receiver front end and ZFE detector.

We collect sets of $M$ of these scalar measurements to form the vector $\mathbf{y}(n) = [y_1(n), \ldots, y_M(n)]^T$ with the MIMO model

$$\mathbf{y}(n) = \sum_{k=-\infty}^{\infty} A_{l_{n-k}} \mathbf{H}(k) \mathbf{b}_{l_{n-k}} + \mathbf{n}(k), \tag{89}$$

where $\mathbf{b}_m$ is the $m$th column of the identity matrix and $\mathbf{n}(k)$ is a wide-sense stationary, multivariate, Gaussian random process with correlation sequence $E[\mathbf{n}(k)\mathbf{n}^*(k-n)] = \sigma^2 \mathbf{H}(n)$ and power spectral density $\sigma^2 \mathbf{H}(e^{jw})$. The MIMO channel coefficients, $\mathbf{H}(k)$, are terms in the matrix-valued deterministic channel-correlation sequence

$$\{\mathbf{H}(k)\}_{i,j} = \int_{-\infty}^{\infty} \overline{s_i}(t - kT) s_j(t)\, dt, \tag{90}$$

and form a positive semidefinite sequence in $\ell_2^M$ whenever each continuous time waveform satisfies $s_m(t) \in L_2(\mathbb{R})$. This process is shown in Fig. 11, together with the equalizer and decision branches of the receiver.

### 9.2. *Equalization of the MIMO system*

We will develop a zero-forcing equalizer for use on the noncoherent channel. We caution that decision-feedback equalization of the sort developed for the baseband channel in [26] can not be employed on this channel since the phase and possibly amplitude uncertainty at the receiver prohibit the reconstruction of past signals.

When the MIMO filter, $\{\mathbf{H}(n)\}$, is invertible we can completely remove the ISI by applying the inverse filter $(\mathbf{Q}(e^{j\theta}) = \mathbf{H}^{-1}(e^{j\theta})$, where $\mathbf{H}(e^{j\theta}) = \sum \mathbf{H}(k) e^{j\theta k})$ as in [3] to obtain the ISI-free output sequence $\{\mathbf{z}(n)\}$:

$$\mathbf{z}(n) = (\{\mathbf{Q}\} * \{\mathbf{y}\})(n) = A_{l_n} \mathbf{b}_{l_n} + \mathbf{w}(n). \tag{91}$$

The noise vector $\mathbf{w}(n)$ has the MIMO correlation sequence $E[\mathbf{w}(n)\mathbf{w}^*(n-k)] = \sigma^2\{\mathbf{Q}\}(k)$. The resulting post-equalizer detector will make decisions on each output independently.

In order to match the post-equalizer model with that of Section 3 consider the equivalent statistic $\mathbf{x}(n) = \mathbf{Q}(0)^{1/2}\mathbf{z}(n)$, where $\mathbf{Q}(0)^{1/2}$ is a positive definite square root of the matrix $\mathbf{Q}(0)$. The model becomes

$$\mathbf{x} = A_l \mathbf{Q}(0)^{1/2}\, \mathbf{b} + \mathbf{q}, \tag{92}$$

where $\mathbf{q}$ is a zero-mean Gaussian random vector with correlation $\sigma^2 \mathbf{I}$ and we have suppressed the time dependency since we are performing one-shot detection. Out model now matches that of Sections 3 and 4 (and Section 8 in the case of a Rayleigh fading channel) and the detectors derived there may be employed.

### 9.3. *Numerical Example*

We consider a system in which 4-ary FSK signaling is employed over a multipath channel with 3 discrete multi-paths. The channel impulse response is given by

$$h(t) = \sum_{n=1}^{N} \beta_n \delta(t - \tau_n), \tag{93}$$

with $N = 3$ paths described by $\{\beta_n\} = \{-0.480 + 0.230j,\ 0.190 + 0.272j,\ -0.133 + 0.237j\}$, $\{\tau_n\} = \{0.058T, 0.353T, 0.813T\}$, and $T = 1/9600$ s. For this example, the equivalent length 3 FIR discrete-time MIMO channel is invertible, and the resulting probability of error plots for the AO and the GML detectors

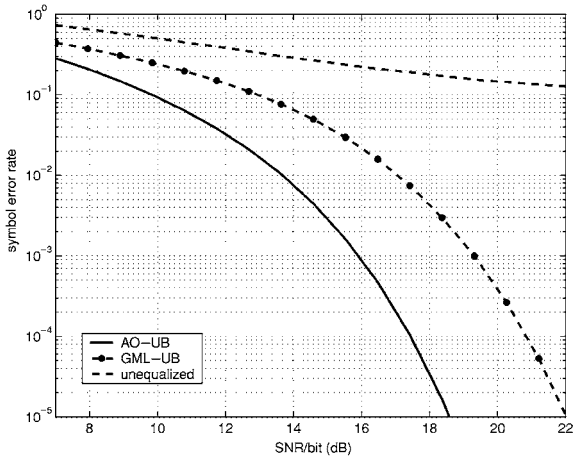


*Figure 12.* Probability of error for 4-ary FSK over the ISI channel of Eq. (93).

are shown in Fig. 12. Notice that for this example, the AO detector outperforms the GML detector by about 5 dB. This is due to the large difference in energies in the signals after equalization. For comparison, we also plot the probability of error for the non-equalized system with conventional noncoherent envelope detection without equalization. For a given realization of the phase terms, $\{\theta_k\}_{k=-1}^{1}$, we compute the union bound on the probability of error for this detector as in Section 4. A Monte-Carlo average of the resulting union bound is taken over the uniform distribution of the phase terms. It is clear that ignoring the effects of the ISI are catastrophic for this channel.

## 10. Summary

We have presented a comprehensive development of NMM signaling on the noncoherent AWGN channel including detection, signal design, coding, and equalization. Several examples were included which indicated the performance advantages enjoyed by NMM over orthogonal modulation schemes such as FSK with respect to bandwidth efficiency. We presented an outline of the extension of these ideas to the Rayleigh fading channel. There is also a rich multi-user detection theory of NMM on the noncoherent channel which has been developed in [1, 2, 27–33].

## References

1. M.K. Varanasi and A. Russ, "Noncoherent Decorrelative Detection for Nonorthogonal Multipulse Over the Multiuser Gaussian Channel," *IEEE Trans. Commun.*, vol. 46, no. 12, 1998, pp. 1675–1684.
2. M.L. McCloud and L.L. Scharf, "Interference Estimation with Applications to Blind Multiple-Access Communication Over Fading Channels," *IEEE Trans. Inform. Theory*, vol. 46, no. 3, 2000, pp. 947–961.
3. M.K. Varanasi, "Noncoherent Equalization for Multipulse Modulation," in *Proc. IEEE Personal, Indoor and Mobile Communications Conf.*, Boston, MA, Sept. 1998.
4. M.K. Varanasi and M.L. McCloud, "Complex Spherical Modulation for Non-Coherent Communications," in *Proc. IEEE Intl. Symposium on Information Theory*, Sorrento, Italy, June 2000, p. 163.
5. C.T. Lawrence, J.L. Zhou, and A.L. Tits, *User's Guide for CFSQP Version 2.5: A C Code for solving (Large Scale) Constrained Nonlinear (Minimax) Optimization Problems, Generating Iterates Satisfying All Inequality Constraints*, College Park, MD: University of Maryland, 1997.
6. W.E. Stark, "Capacity and Cutoff Rate of Noncoherent FSK with Nonselective Rician Fading," *IEEE Trans. Commun.*, vol. 33, no. 11, 1985, pp. 1153–1159.
7. W.E. Ryan and S.G. Wilson, "Two Classes of Convolutional Codes Over GF(q) for q-ary Orthogonal Signaling," *IEEE Trans. Commun.*, vol. 39, no. 1, 1991, pp. 30–40.
8. M. Brehler and M.K. Varanasi, "Asymptotic Error Probability Analysis of Quadratic Receivers in Rayleigh Fading Channels with Applications to a Unified Analysis of Coherent and Noncoherent Space-Time Receivers," *IEEE Trans. Inform. Theory*, vol. 47, no. 5, pp. 2383–2399, 2001.
9. M.L. McCloud, M. Brehler, and M.K. Varanasi, "Signal Design and Convolutional Coding for Noncoherent Space-Time Communication on the Rayleigh Fading Channel," *IEEE Trans. Inform. Theory*, submitted.
10. E.A. Lee and D.G. Messerschmitt, *Digital Communication*, 2nd edn., Boston, MA: Kulwer Academic Publishers, 1994.
11. M. Varanasi, "Equalization for Multipulse Modulation," in *Proc. 1997 IEEE Intl. Conf. on Personal Wireless Communications (ICPWC'97)*, Mumbai (Bombay), India, Dec. 1997, pp. 48–51.
12. M. McCloud and M. Varanasi, "Noncoherent Zero Forcing Equalization for Multipluse Modulation," in *Proc. Conf. Inform. Sciences and Systems*, Princeton, NJ, March 2000, Princeton University, pp. FP2.1–FP2.6.
13. M.L. McCloud and M. Varanasi, "Noncoherent Zero Forcing and Decision Feedback Equalization for Multipulse Modulation," *IEEE Trans. Inform. Theory*, submitted.
14. H.V. Poor, *Introduction to Signal Detection and Estimation*, New York: Springer-Verlag, 1994.
15. L.L. Scharf, *Statistical Signal Processing*, Reading, MA: Addison-Wesley, July 1991.
16. M.K. Varanasi and A. Russ, "Noncoherent Decorrelative Multiuser Detection for Nonlinear Nonorthogonal Modulation," in *Proc. IEEE Intl. Conf. on Communications*, Montreal, Canada, June 1997, pp. 919–923.
17. I.N. Bronstein and K.A. Semendyayev, *Handbook of Mathematics*, 3rd edn. Verlag Harri Deutsch, Thun and Frankfurt/Main, 1985.
18. J.G. Proakis, *Digital Communications*, 3rd edn., New York: McGraw-Hill, 1995.
19. M.K. Varanasi, "Noncoherent Detection in Asynchronous Multiuser Channels," *IEEE Trans. Inform. Theory*, vol. 39, no. 1,

1993, pp. 157–176.
20. R. Pawula, "Relations Between the Rice Ie-Function and the Marcum Q-Function with Applications to Error Rate Calculations," *Electronics Letters*, vol. 31, no. 24, 1995, pp. 2078–2080.
21. I.S. Gradshteyn and I.M. Ryzhik, *Table of Integrals, Series, and Products*, 4th edn., New York: Academic Press, 1965.
22. L. Welch, "Lower Bounds on the Maximum Cross Correlation of Signals," *IEEE Trans. Inform. Theory*, vol. 20, no. 3, 1974, pp. 397–399.
23. G. Ungerboeck, "Channel Coding with Amplitude/Phase Signals," *IEEE Trans. Inform. Theory*, vol. 28, no. 1, 1982, pp. 55–65.
24. M. Schwartz, W.R. Bennett, and S. Stein, *Communication Systems and Techniques*, Reissue, New York: IEEE Press Classic, 1996 (Originally A McGraw-Hill Publication, 1996).
25. M. Loeve, *Probability Theory*, New York, NY: Springer-Verlag, 1977.
26. A. Duel-Hallen, "Equalizers for Multiple Input/Muliple Output Channels and PAM Systems with Cyclostationary Input Sequences," *IEEE Journal on Selected Areas in Commun*., vol. 10, no. 3, 1992, pp. 630–639.
27. M.K. Varanasi and D. Das, "Noncoherent Decision Feedback Multiuser Detection: Optimality, Performance Bounds, and Rules for Ordering Users," in *Proc. IEEE Intl. Symposium on Information Theory*, Aug. 1998, p. 35.
28. M.K. Varanasi and D. Das, "Noncoherent Decision Feedback Multiuser Detection," *IEEE Trans. Commun*., vol. 48, no. 2, 2000, pp. 259–269.
29. M.L. McCloud and L.L. Scharf, "Asymptotic Analysis of the MMSE Multiuser Detector for Non-Orthogonal Multipulse Modulation," *IEEE Trans. Commun*., vol. 49, no. 1, 2001, pp. 24–30.
30. A. Kapur, D. Das, and M.K. Varanasi, "Noncoherent MMSE Multiuser Receivers for Non-Orthogonal Multipulse Modulation and Blind Adaptive Algorithms," *IEEE Trans. Commun*, to appear.
31. A. Russ and M.K. Varanasi, "Noncoherent Multiuser Detection for Nonlinear Modulation Over the Rayleigh Fading Channel," *IEEE Trans. Inform. Theory*, vol. 47, no. 1, 2001, pp. 295–307.
32. E. Visotsky and U. Madhow, "Noncoherent Multiuser Detection for CDMA Systems with Nonlinear Modulation: A Non-Bayesian Approach," *IEEE Trans. Inform. Theory*, vol. 47, no. 4, 2001, pp. 1352–1367.
33. A. Russ and M.K. Varanasi, "An Error Probability Analysis of the Optimum Noncoherent Multiuser Detector for Nonorthogonal Multipulse Modulation Over the Frequency-Selective Rayleigh Fading Channel," *IEEE Trans. Commun*., submitted.

**Michael McCloud** received the B.S. degree in Electrical Engineering from George Mason University, Fairfax, VA in 1995 and the M.S. and Ph.D. degrees from in electrical Engineering from the University of Colorado in 1998 and 2000, respectively.

He spent the 2000–2001 academic year as a Visiting Researcher and Lecturer at the University of Colorado. He has been a Senior Engineer with Magis Networks, San Diego, CA since May, 2001. His research interests include statistical signal processing and wireless communication theory.
mccloud@ieee.org

**Mahesh K. Varanasi** received his B.E. degree in Electronics and Communications Engineering from Osmania University, Hyderabad, India in 1984 and the M.S. and Ph.D. degrees in Electrical Engineering from Rice University, Houston, TX, in 1987 and 1989, respectively.

In 1989, he joined the faculty of the University of Colorado at Boulder where he is now Professor of Electrical and Computer Engineering. His teaching and research interests are in the areas of communication theory, information theory and signal processing. His research contributions have been in the areas of multiuser detection, space-time communications, equalization, signal design and power control for multiple-access, fading channels and diversity systems, blind receivers, and power and bandwidth-efficient multiuser communications. He was elected Senior Member of IEEE in 1995.
varanasi@schof.colorado.edu